International Journal of Fluid Mechanics Research, 46(6):565–578 (2019)

ON THE V2-BASED TURBULENCE MODEL FOR FREE-STREAM AND WALL-BOUNDED HIGH-SPEED COMPRESSIBLE FLOWS

Alexander M. Molchanov, Dmitry S. Yanyshev,* Leonid V. Bykov, & Ivan M. Platonov

Aerospace Heating Engineering Department, Moscow Aviation Institute (National Research University) "MAI," Moscow, Russia

*Address all correspondence to: Dmitry S. Yanyshev, Aerospace Heating Engineering Department, Moscow Aviation Institute (National Research University) "MAI," Volokolamskoe shosse, d. 4, 125993, Moscow, Russia; Tel.: +7 499 158 0027; Fax: +7 499 158 2977, E-mail: dyanishev@gmail.com

Original Manuscript Submitted: 2/20/2018; Final Draft Received: 5/18/2018

A turbulence model for free-stream and wall-bounded high-speed compressible flows is presented. The core of the model is based on the assumption that the key role in turbulent mixing processes is played by velocity fluctuations normal to streamlines. Thus a separate partial differential equation is solved to model this parameter correctly. Effect of compressibility is handled via modeling the rapid part of pressure-strain correlation depending on turbulent Mach number. To model turbulence in the near-wall region, a blending technique is used (similar to the one introduced in Menter's SST model). The developed model is verified in free-stream and wall-bounded conditions. Comparison of the simulation with available experimental data showed a good agreement for the above problems.

KEY WORDS: *turbulence, compressibility, CFD, semi-empirical models, Navier–Stokes equations*

1. INTRODUCTION

Turbulent flow is often prevailing in modern vehicles and machinery. Turbulence is one of the underlying phenomena in fluid dynamics and heat transfer. The phenomenon of turbulence was discovered more than a century ago, yet it has not been fully understood. One of the biggest problems that remain in this area is investigation of turbulent gas flow at high speeds.

As it is known, one of the main features of any gas medium is compressibility. In certain conditions (generally characterized by the magnitude of Mach number), compressibility is starting to affect the flow parameters greatly. The growth rate of turbulent kinetic energy is critically reduced with the increase of turbulent Mach number. Compressibility in high-speed flows has a stabilizing effect on turbulence so that the intensity of turbulent mixing reduces as Mach number increases.

A typical supersonic effect is a drastic reduction in the growth rate of a plane free-shear layer flow. The reduction was confirmed in plenty of experiments under various conditions (e.g., see Goebel and Dutton, 1991; Kline et al., 1981; Krasotkin et al., 1988; Lau et al., 1979; Papamoschou and Roshko, 1988).

This effect plays an important role in present-day problems of rocket and airspace engineering. For example, in a supersonic combustion ramjet, reduced turbulence levels can be highly detrimental, as they reduce the rate of fuel and oxidizer mixing. Compressibility changes the nature of boundary-layer transition to turbulence in flows over hypersonic vehicles during reentry.

Nevertheless, it must be noted that in some cases, compressibility makes a very small impact on turbulence. For example, the experimental data obtained by Goebel and Dutton (1991), Mathur and Dutton (1996), and Dutton and

2152-5102/19/$35.00 © 2019 by Begell House, Inc. www.begellhouse.com

Addy (1998) show that axial turbulence intensity actually does not depend on Mach number. Compressibility also has very little impact on the intensity of turbulence in the near-wall region.

In particular, the local density extensions of standard incompressible turbulence models were found to be inadequate in duplicating the experimentally observed reduction in growth rate of the mixing layer with increasing Mach number.

The results of Sarkar (1995), Simone et al. (1997), Zeman (1990), Glebov and Molchanov (1982), Molchanov (2009), and Sarkar et al. (1992) for compressible turbulent flows showed that the compressibility effects are associated with the dilatational terms, such as the dilatation dissipation and the pressure-dilatation correlation. But later the studies of Vreman et al. (1996) confirmed that the dilatational terms couldn't be regarded as essential in causing the reduced growth rate of turbulent kinetic energy. They pointed out that compressibility was found to affect the production term via the pressure–strain correlation. Besides, the models based on supplementing additional dissipation to the equation of turbulent kinetic energy are unable to predict the increasing turbulence anisotropy. The experiments by Goebel and Dutton (1991), Mathur and Dutton (1996), and Dutton and Addy (1998) showed that with increase of Mach number, the cross-stream turbulence fluctuations are affected to a greater extent than the streamwise ones.

The increasing anisotropy of turbulence is confirmed by data of Simone et al. (1997), Blaisdell et al. (1993), and Freund et al. (2000).

Huang and Fu (2008) showed that the main compressibility effect came from the reduced pressure-strain term due to reduced pressure fluctuations. A damping function of turbulent Mach is used to take account of the compressible effects. The pressure-strain correlation in compressible flows is corrected by the damping function of the turbulent Mach number.

Gomez and Girimaji (2011) suggested that compressibility's impact on turbulence only manifests itself via the rapid part of pressure-strain. They use a rapid pressure-strain correlation model developed within their research group over the last few years that is consistent with rapid distortion theory (RDT) (see Bertsch, 2010; Lavin, 2007). They developed an algebraic Reynolds stress model for compressible flows by accounting for the changing nature of pressure at different gradient Mach number M_G regimes and showed that the major impact of compressibility on turbulence is implemented on large-scale levels and is associated with the fact that the effect of pressure is quite different at low- and high-speed regimes. Pressure-strain correlation scrambles the streamwise and stream-normal fluctuations, leading to a low turbulent shear stress and decreased production.

The formulas were obtained for pressure dilatation depending on gradient Mach number and production by Gomez and Girimaji (2011). The results of RDT obtained by Gomez and Girimaji (2011), Lavin (2007), and Bertsch (2010) show that the effect of pressure has three different regimes depending on Mach numbers:

1. In low-speed flows, pressure assumes the role of enforcing incompressibility and is governed by a Poisson equation. A standard incompressible pressure-strain correlation without any modification can be used (denoted as $\Pi_{ij}^{(P)}$).

2. For an intermediate Mach number, both inertial and pressure terms are of the same order of magnitude: $|\Pi_{ij}| \approx |P_{ij}|$. It is shown by Gomez and Girimaji (2011) that this regime leads to a stabilization of the turbulent kinetic energy growth rate.

3. At very high Mach numbers, pressure plays an entirely negligible effect compared to inertial terms such as P_{ij}. Pantano and Sarkar (2002) showed that for high speeds, the finite speed of sound causes a time delay in the transmission of pressure signals in the flow. Therefore, in this regime, we may neglect the dominant terms in the pressure-strain correlation model: ${\Pi_{ij}}^{(2)} \approx 0$.

This article aims:

1. to develop a turbulence model for high-speed compressible flows on the basis of modeling of the rapid part of pressure-strain correlation depending on turbulent Mach number;

2. to come up with a versatile model that will be applicable to both free shear flows (jets, mixing layers, etc.) and the wall-bounded ones.

As it has been mentioned earlier in this article, the impact of compressibility is of low significance in the near-wall region. Thus, to accomplish the aims described above, a modular approach could be utilized. In the first stage, free-stream turbulence is to be considered independently and an appropriate model is to be developed. In the second stage, the near-wall region is to be "plugged" into the model developed in the previous stage.

2. FREE-STREAM TURBULENCE MODEL

First of all, as a basis, let us consider the Reynolds stress transport equation (see Kollmann, 1980):

$$\frac{\partial}{\partial t}\left(\bar{\rho}\widetilde{u_i{}'u_j{}'}\right)+\frac{\partial}{\partial x_k}\left(\bar{\rho}\tilde{u}_k\widetilde{u_i{}'u_i{}'}\right)=T_{ijk.k}+P_{ij}+\Pi_{ij}-\bar{\rho}\varepsilon_{ij} \tag{1}$$

where

$$\begin{aligned}
T_{ijk.k}&=\frac{\partial}{\partial x_k}\left(-\overline{\rho u_k{}'u_i{}'u_j{}'}+\overline{u_i{}'\tau_{jk}}+\overline{u_j{}'\tau_{ik}}-\delta_{kj}\overline{p'u_i{}'}-\delta_{ki}\overline{p'u_j{}'}\right)\\
P_{ij}&=-\left(\overline{\rho u_i{}'u_k{}'}\frac{\partial\widetilde{u_j}}{\partial x_k}+\overline{\rho u_j{}'u_k{}'}\frac{\partial\widetilde{u_i}}{\partial x_k}\right)\\
\Pi_{ij}&=\left(\overline{p'\frac{\partial u_i{}'}{\partial x_j}}+\overline{p'\frac{\partial u_j{}'}{\partial x_i}}\right)\\
\varepsilon_{ij}&=\frac{2}{3}\varepsilon\delta_{ij}
\end{aligned}$$

Pressure-strain correlation Π_{ij} is divided into the slow, $\Pi_{ij}^{(1)}$, and rapid, $\Pi_{ij}^{(2)}$, parts:

$$\Pi_{ij}=\Pi_{ij}^{(1)}+\Pi_{ij}^{(2)} \tag{2}$$

It is assumed that the slow part $\Pi_{ij}^{(1)}$, which has the physical sense of the tendency toward isotropy and is associated with small-scale turbulence, can be expressed by the formula, which is valid for an incompressible flow (see Kollmann, 1980),

$$\Pi_{ij}^{(1)}=-C_1\bar{\rho}\varepsilon\left(\frac{\widetilde{u_i'u_j'}}{K}-\frac{2}{3}\delta_{ij}\right) \tag{3}$$

where $C_1=1.8$. The rapid part $\Pi_{ij}^{(2)}$ is associated with large-scale turbulence.

The results of rapid distortion theory (RDT) obtained by Gomez and Girimaji (2011), Lavin (2007), and Bertsch (2010) show that the following formula can be used for the rapid part of the pressure-strain correlation $\Pi_{ij}^{(2)}$:

$$\Pi_{ij}^{(2)}=C_{\Pi1}\Pi_{ij}^{(P)}-C_{\Pi2}P_{ij} \tag{4}$$

where $C_{\Pi1}, C_{\Pi2}$ are functions of the gradient Mach number M_g having the following form:

$$\begin{aligned}
M_g<\alpha:&\quad\begin{cases}C_{\Pi1}=1\\C_{\Pi2}=0\end{cases}\\
\alpha\le M_g\le:&\quad\begin{cases}C_{\Pi1}\to 0\\C_{\Pi2}\to 1\end{cases}\\
\beta<M_g:&\quad\begin{cases}C_{\Pi1}=0\\C_{\Pi2}=0\end{cases}
\end{aligned} \tag{5}$$

where α and β are some constants.

In this article, a similar approach is used. However, instead of gradient Mach number M_g, another criterion is used, and thus functions $C_{\Pi 1}$, $C_{\Pi 2}$ are modified accordingly (the details will be given later).

For modeling $\Pi_{ij}^{(P)}$, the simple formula obtained by Kollmann (1980) is used:

$$\Pi_{ij}^{(P)} = -C_2 \left(P_{ij} - \frac{2}{3} P \delta_{ij} \right) \tag{6}$$

where constant $C_2 = 0.6$.

Using given assumptions and taking a trace of Eq. (1) we can obtain the following form of the K-equation:

$$\frac{\partial}{\partial t} \left(\bar{\rho} K \right) + \frac{\partial}{\partial x_k} \left(\bar{\rho} \tilde{u}_k K \right) = T_{k.k} + P \left(1 - C_{\Pi 2} \right) - \bar{\rho} \varepsilon \tag{7}$$

where $P = (1/2) P_{ii} = \overline{\rho u_i' u_k'} [(\partial \tilde{u}_i)/(\partial x_k)]$, production on of turbulent kinetic energy. Thus, dilatational terms in the equation for turbulent kinetic energy are expressed via $C_{\Pi 2}\left(M_T\right) \cdot P$—the product of function of turbulent Mach number and production term.

It is supposed that the equation for turbulent dissipation rate ε has almost standard form and need only be slightly modified to be consistent with a suppressing effect of compressibility on the production term:

$$\frac{\partial}{\partial t} \left(\bar{\rho} \varepsilon \right) + \frac{\partial}{\partial x_k} \left(\bar{\rho} \tilde{u}_k \varepsilon \right) = \frac{\partial}{\partial x_k} \left[\left(\mu + \frac{\mu_T}{\sigma_\varepsilon} \right) \frac{\partial \varepsilon}{\partial x_k} \right] + \frac{\varepsilon}{K} \left[C_{\varepsilon 1} P \left(1 - C_{\Pi 2} \right) - C_{\varepsilon 2} \bar{\rho} \varepsilon \right] \tag{8}$$

The next key step in developing the model is to obtain a proper formula for eddy viscosity.

As it can be seen from dimensional analysis, $\mu_T \sim \rho \mathcal{V}^2 \mathcal{T}$, where $\mathcal{V}$ and $\mathcal{T}$ are turbulent velocity and time scales, correspondingly. Let us consider the velocity scale (the time scale will be determined later).

The classical approach is to use $\mathcal{V} = \sqrt{K}$. However, as noted by Durbin (1991), the more physically and mathematically precise formula is $\mathcal{V} = V_n'$, where V_n' is velocity fluctuation normal to streamlines.

The following simple physical reasoning could be provided for that. In laminar flow, molecular viscosity is responsible for momentum transfer between flow layers. Eddy viscosity is the turbulent analog of molecular viscosity; therefore it is also responsible for transfer of momentum in the same direction. The main momentum transfer in the flow usually occurs across its streamlines (between layers of fluid with different speed). The main mechanism of momentum transfer in turbulent flow is through eddies, which cause velocity fluctuations. Thus, the eddy momentum transfer coefficient should be proportional to the velocity fluctuations normal to streamlines.

In a lot of cases, $K \approx V_n'^2$; however, it is not always true, so $V_n'^2$ needs to be somehow determined.

Let's consider a 2D flow in which the coordinate with a subscript "1" is directed along the streamline and the index "2" denotes the coordinate normal to the streamline. Obviously, the following is true in this case:

$$\tilde{u_2} \ll \tilde{u_1}, \quad \frac{\partial f}{\partial x_1} \ll \frac{\partial f}{\partial x_2}, \quad f = \tilde{u_1}, \tilde{u_2}, \quad \tilde{u_3} = 0, \quad \frac{\partial f}{\partial x_3} = 0 \tag{9}$$

Then, from (1):

$$P_{12} \approx -\overline{\rho u_2' u_2'} \frac{\partial \tilde{u_1}}{\partial x_2}, \quad P_{22} \approx 0, \quad P_{11} \approx -2 \overline{\rho u_1' u_2'} \frac{\partial \tilde{u_1}}{\partial x_2}, \quad P \approx -\overline{\rho u_1' u_2'} \frac{\partial \tilde{u_1}}{\partial x_2} \tag{10}$$

Using Eqs. (1), (3), (4), and (6) and assumption (10), we obtain the following equation for $\widetilde{u_2'^2} = \widetilde{V_n'^2}$:

$$\frac{\partial}{\partial t} \left(\bar{\rho} \widetilde{V_n'^2} \right) + \frac{\partial}{\partial x_k} \left(\bar{\rho} \tilde{u}_k \widetilde{V_n'^2} \right) = \frac{\partial}{\partial x_k} \left[\left(\mu + \frac{\mu_T}{\sigma_K} \right) \frac{\partial \widetilde{V_n'^2}}{\partial x_k} \right] + \frac{2}{3} C_{\Pi 1} C_2 P - \left[C_1 \frac{\widetilde{V_n'^2}}{K} + \frac{2}{3} \left(1 - C_1 \right) \right] \bar{\rho} \varepsilon \tag{11}$$

Let us consider the source term in the equation for shear stress [Eq. (1) with $i = 1$, $j = 2$]:

$$S_{12} = -\left(1 - C_{\Pi 2} - C_{\Pi 1} C_2 \right) \rho \widetilde{u_2' u_2'} \frac{\partial \tilde{u_1}}{\partial x_2} - C_1 \frac{\widetilde{u_1' u_2'}}{K} \rho \varepsilon \tag{12}$$

Hossain (1980) and Ljuboja and Rodi (1980), considering algebraic stress models, showed that convective and diffusive transfer in the differential equation for shear stress could be neglected, that is, $S_{12} \approx 0$. Thus, from formula (12), we obtain an explicit expression for the shear stress:

$$\widetilde{u_1' u_2'} = -\frac{(1 - C_{\Pi 1} C_2 - C_{\Pi 2})}{C_1} \frac{K}{\varepsilon} \widetilde{u_2' u_2'} \frac{\partial \widetilde{u_1}}{\partial x_2} \tag{13}$$

From Eq. (13), we obtain a formula for the shear stress in the familiar form:

$$\bar{\rho} \widetilde{u_1' u_2'} = -\mu_T \frac{\partial \widetilde{u_1}}{\partial x_2} \tag{14}$$

where the eddy viscosity is given by

$$\mu_T = \frac{(1 - C_{\Pi 1} C_2 - C_{\Pi 2})}{C_1} \bar{\rho} \widetilde{V_n'^2} \frac{K}{\varepsilon}, \tag{15}$$

It is assumed that the eddy viscosity obtained via formula (15) can be applied to all components of Reynolds stress, and in the general case, the following classical formula is true in the case of compressible flow:

$$-\bar{\rho} \widetilde{u_i' u_j'} = \mu_T \left(\frac{\partial \tilde{u}_i}{\partial x_j} + \frac{\partial \tilde{u}_j}{\partial x_i} \right) - \frac{2}{3} \delta_{ij} \mu_T \frac{\partial \tilde{u}_m}{\partial x_m} - \frac{2}{3} \delta_{ij} \bar{\rho} K \tag{16}$$

Model coefficients are provided in Table 1. Summing up, the free-stream model consists of Eqs. (7), (8), and (11). It was tested in several test-cases. The results of the validation are given by Molchanov and Bykov (2013).

3. TAKING INTO ACCOUNT THE NEAR-WALL REGION

It is a well-known fact that the ε-equation in its classical form is not suitable for modeling wall-bounded flows. When using ε-equation based turbulence models, several approaches are available for correct resolving of the near-wall region:

1. implementation of damping functions;
2. blending the ε-equation with the ω-equation, as the ω-equation is "good" for wall-bounded flows but could be inadequate for free-stream flows;
3. using elliptic-relaxation function to model near-wall effects like Durbin (1991) and Manceau and Hanjalic (2002).

The third option seems the most interesting and physically justified.

However, when using Durbin's v^2-f model (see Durbin, 1991) for complex flows, there appear problems with boundary conditions on the wall. Simulation results turn out to be very grid-sensitive in the near-wall region (see Jones, 1996).

The model described by Manceau and Hanjalic (2002) was actually implemented within this study previously (see Molchanov and Bykov, 2013). However, the predictions it gave went worse with the experimental data in comparison with the SST-like model.

Another problem with elliptic-relaxation models lies in unsteady flow modeling: the models could show non-physical behavior in unsteady flow conditions (see Kraev and Yanyshev, 2014). This could be due to some properties

TABLE 1: K-ε-V_n model coefficients

σ_K	σ_ε	$C_{\varepsilon 1}$	$C_{\varepsilon 2}$	C_1	C_2
1.0	1.3	1.44	1.92	1.8	0.6

of the elliptic-relaxation function equation, which lacks a transient term. However, for now, it is uncertain whether this problem is just a numerical effect or lies in physics.

Consequently, in the present work, the blending approach was chosen to deal with the near-wall region.

Modern well-known blending-based models [e.g. Menter's SST, see Menter (1994)] usually imply using ε- and ω-equations.

However, the ω-equation has a certain disadvantage connected with determining wall boundary conditions as on the wall surface $\omega \to \infty$, which creates certain handicaps for numerical solutions. In the present work the omega equation is replaced by an equation for g-parameter determined as

$$g^2 = 1/(\beta^* \omega), \quad g^2 = K/\varepsilon \tag{17}$$

This approach was initially used by Kalitzin et al. (1994).

Using g-parameter, being the square root of turbulence time scale, grants natural boundary conditions on the wall, $g_w = 0$.

Blending is performed by transforming the ε-equation into the g-equation with formula (17) and using blending functions [the same approach is utilized in the SST model (Menter, 1994)].

Omitting trivial computations, let us write the system of equations of the model:

$$\frac{\partial}{\partial t}(\rho K) + \frac{\partial}{\partial x_k}(\overline{\rho}\tilde{u}_k K) = \frac{\partial}{\partial x_k}\left[\left(\mu + \frac{\mu_T}{\sigma_K}\right)\frac{\partial K}{\partial x_k}\right] + P^* - \frac{\rho K}{g^2} \tag{18}$$

$$\begin{aligned}\frac{\partial}{\partial t}(\overline{\rho} g) + \frac{\partial}{\partial x_k}(\overline{\rho}\tilde{u}_k g) = {} & \frac{\partial}{\partial x_k}\left[\left(\mu + \frac{\mu_T}{\sigma_g}\right)\frac{\partial g}{\partial x_k}\right] \\ & - \frac{\alpha}{2}\frac{g}{K}P^* + \frac{\beta\rho}{2\beta^* g} - \frac{3}{g}\left(\mu + \frac{\mu_T}{\sigma_g}\right)\frac{\partial g}{\partial x_k}\frac{\partial g}{\partial x_k} \\ & + \frac{(1-F_1)}{K}\left\{\frac{2\mu_T}{\sigma_g}\frac{\partial K}{\partial x_k}\frac{\partial g}{\partial x_k} + \frac{g}{2}\frac{\partial}{\partial x_k}\left[\mu_T\left(\frac{1}{\sigma_K} - \frac{1}{\sigma_\varepsilon}\right)\frac{\partial K}{\partial x_k}\right]\right\}\end{aligned} \tag{19}$$

$$\begin{aligned}\frac{\partial}{\partial t}\left(\overline{\rho}\widetilde{V_n'^2}\right) + \frac{\partial}{\partial x_k}\left(\overline{\rho}\tilde{u}_k\widetilde{V_n'^2}\right) = {} & \frac{\partial}{\partial x_k}\left[\left(\mu + \frac{\mu_T}{\sigma_K}\right)\frac{\partial \widetilde{V_n'^2}}{\partial x_k}\right] \\ & + \frac{2}{3}C_{\Pi 1}C_2 P - \left[C_1\frac{\widetilde{V_n'^2}}{K} + \frac{2}{3}(1 - C_1)\right]\frac{\rho K}{g^2}\end{aligned} \tag{20}$$

$$\mu_T = \min\left(C_D\rho\widetilde{V_n'^2}g^2; \frac{\rho a_1 K}{SF_2}\right) \tag{21}$$

where $a_1 = 0.31$ is a Bradshaw constant and blending functions are defined as follows:

$$\begin{gathered}F_1 = \tanh\left(\arg_1^4\right); \quad \arg_1 = \min\left[\max\left(\frac{g^2\sqrt{K}}{y}, \frac{500\mu\beta^* g^2}{\rho y^2}\right), \frac{1}{CD_{K\omega}}\frac{4\rho K}{\sigma_\varepsilon y^2}\right] \\ CD_{K\omega} = \max\left(-\frac{4\rho}{\sigma_\varepsilon g}\frac{\partial K}{\partial x_j}\frac{dg}{dx_j}, 1.0\times 10^{-10}\right); \quad F_2 = \tanh\left(\arg_2^2\right) \\ \arg_2 = \max\left(2\frac{g^2\sqrt{K}}{y}, \frac{500\mu\beta^* g^2}{\rho y^2}\right)\end{gathered} \tag{22}$$

Model coefficients are defined using blending functions:

$$\begin{aligned}
\alpha &= F_1\alpha_1 + (1-F_1)(C_{\varepsilon 1}-1)\\
\frac{\beta}{\beta^*} &= F_1\frac{\beta}{\beta^*} + (1-F_1)(C_{\varepsilon 1}-1)\\
\frac{1}{\sigma_g} &= F_1\frac{1}{\sigma_{g1}} + (1-F_1)\frac{1}{\sigma_\varepsilon}\\
\frac{1}{\sigma_K} &= F_1\frac{1}{\sigma_{K1}} + (1-F_1)\frac{1}{\sigma_{K2}}\\
C_D &= F_1\frac{(1-C_2)}{C_1} + (1-F_1)\frac{(1-C_{\Pi 1}C_2 - C_{\Pi 2})}{C_1}
\end{aligned} \tag{23}$$

Values of $C_{\varepsilon 1}$, $C_{\varepsilon 1}$, σ_ε and σ_{K2}, C_1, C_2 are taken as per Table 1 (to be precise, σ_{K2} is taken as σ_K in the table). Other coefficients are taken as per Table 2.

The turbulence source term is modified as stated below (which is a result of the blending procedure as well):

$$P^* = P\left[1-(1-F_1)\,C_{\Pi 2}\right] \tag{24}$$

Functions $C_{\Pi 1}$ and $C_{\Pi 2}$, as it was stated earlier in this article, depend on turbulent Mach number M_T:

$$C_{\Pi 1}(M_T) = \begin{cases} 1, & M_T \le \alpha_{\Pi 1} \\ 1-3\zeta^2+2\zeta^3, & \zeta = \dfrac{(M_T-\alpha_{\Pi 1})}{(\beta_{\Pi 1}-\alpha_{\Pi 1})}, \quad \alpha_{\Pi 1} < M_T < \beta_{\Pi 1} \\ 0, & M_T \ge \beta_{\Pi 1} \end{cases}$$

$$C_{\Pi 2}(M_T) = \begin{cases} C_{\Pi 2,\max}(3\zeta^2+2\zeta^3), & \zeta = \dfrac{(M_T-\alpha_{\Pi 2})}{(\beta_{\Pi 2}-\alpha_{\Pi 2})}, \quad \alpha_{\Pi 2} < M_T \le \beta_{\Pi 2} \\ C_{\Pi 2,\max}(1-3\zeta^2+2\zeta^3), & \zeta = \dfrac{(M_T-\beta_{\Pi 2})}{(\gamma_{\Pi 2}-\beta_{\Pi 2})}, \quad \beta_{\Pi 2} < M_T < \gamma_{\Pi 2} \\ 0, & M_T \le \alpha_{\Pi 2} \cup M_T \ge \gamma_{\Pi 2} \end{cases} \tag{25}$$

$$\alpha_{\Pi 1} = 0.1; \quad \beta_{\Pi 1} = 0.27; \quad \beta_{\Pi 2} = 0.315; \quad \gamma_{\Pi 2} = 10; \quad C_{\Pi 2,\max} = 0.65$$

Turbulent Mach number in this article is defined as follows:

$$M_T = \frac{\min\left(0.2857 L_T S; \sqrt{2K}\right)}{a} \tag{26}$$

where

$$S = \sqrt{2S_{ij}S_{ij}}$$

is invariant of the strain tensor

$$S_{ij} = \frac{1}{2}\left(\frac{\partial u_i}{\partial x_j} + \frac{\partial u_j}{\partial x_i}\right) \quad \text{and} \quad L_T = \min\left(g^2\sqrt{K}; y\right)$$

is a length scale, where y is a distance to the nearest wall.

TABLE 2: K-g-V_n model coefficients

α_1	β^*	β_1	σ_{g1}	σ_{K1}
5/9	0.09	0.075	2.0	1.176

4. MODEL VALIDATION

The model was validated for several flow cases. Experimental flow data of Goebel and Dutton (1991), Fernholz and Finley (1977), Mathur and Dutton (1996), and Dutton and Addy (1998) were used. The calculation results using the present model were also compared with the results obtained using Menter's SST model with compressibility correction by Sarkar et al. (1989) (except for the free stream case, where two versions of the SST model are considered).

Free stream validation was performed using experimental data of Goebel and Dutton (1991). In these experiments, mixing of two parallel gas flows was investigated. The flows had different speed and density. The main parameters of the flows are shown in Table 3 for seven different flow regimes.

Calculation results for the experiment of Goebel and Dutton (1991) are presented in Fig. 1, and in Tables 4 and 5. For this case, two different variants of the SST model were validated: with and without compressibility correction introduced by Sarkar et al. (1989).

TABLE 3: Parameters of the mixing flows based on Goebel and Dutton (1991) used for validation

Regime No.	**1**	**1d**	**2**	**3**	**3r**	**4**	**5**
$r = U_2/U_1$	0.78	0.79	0.57	0.18	0.25	0.16	0.16
$s = \rho_2/\rho_1$	0.76	0.76	1.55	0.57	0.58	0.6	1.14
M_1, M_2	2.01, 1.38	2.02, 1.39	1.91, 1.36	1.96, 0.27	2.22, 0.43	2.35, 0.3	2.27, 0.38
T_1, T_2, [K]	163, 214	151, 198	334, 215	161, 281	159, 275	171, 285	332, 292
U_1, U_2, [m/s]	515, 404	498, 392	700, 399	499, 92	561, 142	616, 100	830, 131
P, [kPa]	46	55	49	53	53	36	32

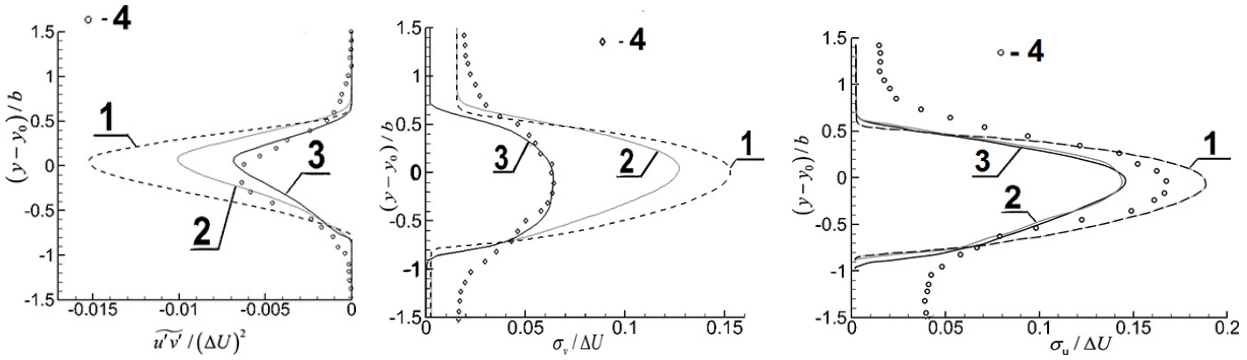

(a) (b) (c)

FIG. 1: Reynolds stress tensor components for mixing of two-dimensional flows computed via different turbulence models [(a) shear stress, (b) fluctuations normal to streamlines, (c) streamwise fluctuations]; 1, SST (no compressibility correction); 2, SST with Sarkar's compressibility correction; 3, present model; 4, experimental data

TABLE 4: Calculation results of the peak of fluctuations normal to streamlines $\sigma_v/(\Delta U)^2$

—	**Regime**						
	1	**1d**	**2**	**3**	**3r**	**4**	**5**
K-g-V_n	0.159	0.15	0.1085	0.08	0.088	0.0066	0.06
SST (no compressibility correction)	0.167	0.16	0.147	0.14	0.154	0.15	0.145
Sarkar SST	0.167	0.157	0.14	0.117	0.154	0.13	0.12
Experimental data	0.15	0.15	0.099	0.078	0.086	0.0066	0.053

TABLE 5: Calculation results of the peak of shear stress $\widetilde{u'v'}/(\Delta U)^2$

—	Regime						
	1	**1d**	**2**	**3**	**3r**	**4**	**5**
K-g-V_n	0.0172	0.0173	0.095	0.068	0.0082	0.0068	0.0064
SST (no compressibility correction)	0.0182	0.0164	0.014	0.012	0.0126	0.0151	0.014
Sarkar SST	0.0174	0.0153	0.0127	0.0086	0.009	0.011	0.009
Experimental data	0.017	0.016	0.086	0.09	0.0073	0.0066	0.0058

By examining these results, we can infer the following. As one can see, increase in relative speed (relative Mach number M_r yields to decrease of shear stress [Fig. 1(a)], considerable decrease of lateral velocity fluctuations [Fig. 1(b)], and to minor alteration of longitudinal fluctuations [Fig. 1(c)].

This means that compressibility, first of all, influences velocity fluctuations normal to streamlines, and through $\overline{V_n'^2}$, on shear stress. At the same time the influence on streamwise fluctuations is negligible. The proposed turbulence model reflects these statements rather well, while SST does not.

For validation of the model in boundary layer conditions, test data by Fernholz and Finley (1977) were used. In this work, near-wall compressible gas flows were investigated. The main flow parameters are presented in Table 6.

The results of calculations are presented in Figs. 2–4.

By considering the obtained results for wall-bounded flow, it is possible to conclude that the present model permits to gain slightly more accurate velocity and temperature profiles, being closer to experimental data.

Another case is investigation of flow field near a blunt cylindrical body with base bleed aligned in a supersonic flow (see Fig. 5). The supersonic free stream expands as it turns the corner, while the turbulent boundary layer separates and then undergoes recompression, realignment, and redevelopment in the wake of the underbody (see Mathur and Dutton, 1996). Fluid from the region adjacent to the base is entrained and accelerated by the outer shear layer and then returned to the base region by a recompression shock system. This region is referred to as the primary recirculation region. Introducing base bleed, the primary recirculation region is moved downstream from the aftbody with a forward stagnation point created, dependent on the relative strengths of the bleed jet and the

TABLE 6: Flow parameters for compressible boundary layer flow based on Fernholz and Finley (1977) used for validation

—	Regime		
	(a)	**(b)**	**(c)**
External flow Mach number, M_e	4.544	2.244	5.29
Relation between wall temperature and reduction temperature, T_w/T_r	1.0	1.0	0.92

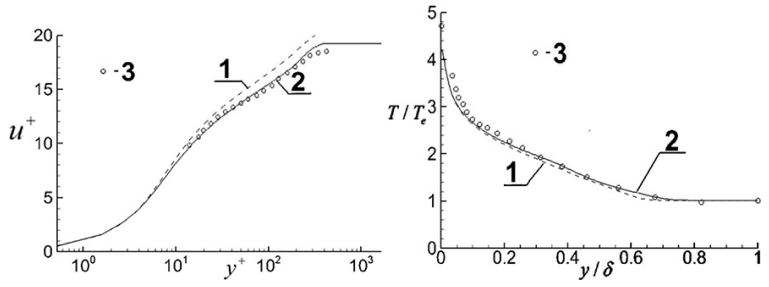

(a) (b)

FIG. 2: Dimensionless velocity $u^+(y^+)$ (a) and temperature profiles (b) for regime (a): 1, results using SST; 2, present model; 3, experimental data

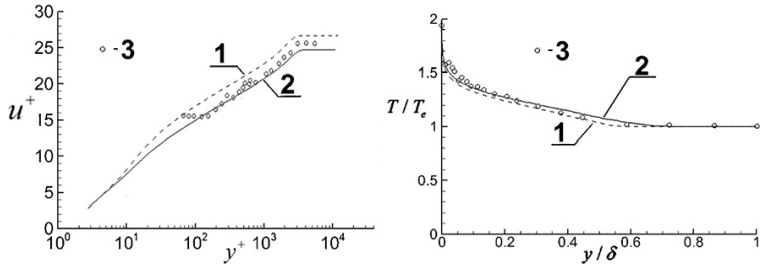

(a) (b)

FIG. 3: Dimensionless velocity $u^+(y^+)$ (a) and temperature profiles (b) for regime (b): 1, results using SST; 2, present model; 3, experimental data

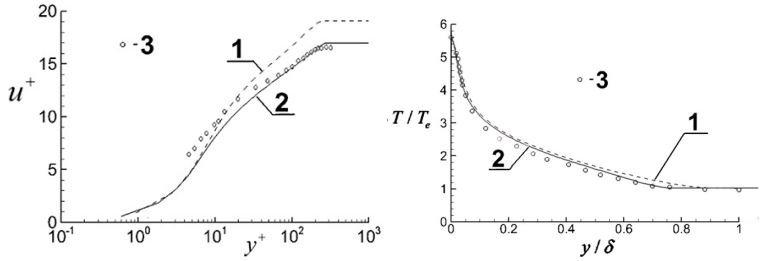

(a) (b)

FIG. 4: Dimensionless velocity $u^+(y^+)$ (a) and temperature profiles (b) for regime (c): 1, results using SST; 2, present model; 3, experimental data

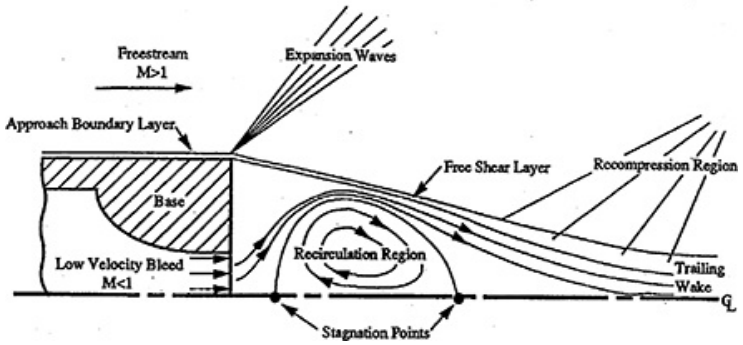

(a)

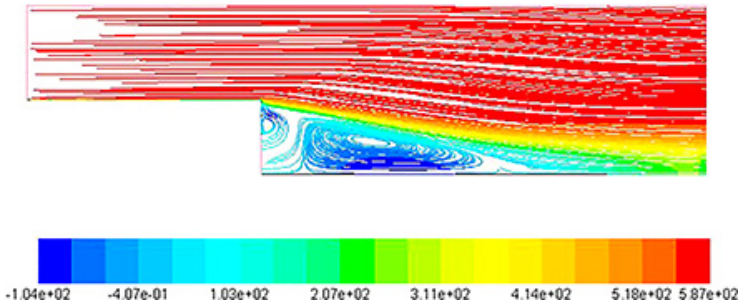

(b)

FIG. 5: Flow field near a blunt cylindrical body with base bleed aligned in a supersonic flow. (a) Schematic diagram of supersonic base flow based on Mathur and Dutton (1996); (b) pathlines colored by axial velocity magnitude (m/s) for $I = 0.01$.

recirculating region. Experiments performed by several investigators [see Dutton and Addy (1998) for a complete list] demonstrated an important effect of such a shift in the location of the primary recirculation region: a change in the base pressure ratio and, a result, a change in the aftbody drag. Base bleed, then, is an effective mechanism for reducing aftbody drag.

The experimental flow conditions are as follows: free stream static pressure $P_e = 28,700$ Pa, free stream Mach number $M_e = 2.47$, tunnel stagnation temperature 300 K, bleed flow mass flow rate ratio $I = 0.01$, base radius 31.75 mm, bleed orifice radius 2.7 mm, bleed flow stagnation temperature 300 K.

Here I is the dimensionless injection parameter:

$$I = \frac{\dot{m}_{\text{bleed}}}{\rho_1 U_1 A_b} \tag{27}$$

where $\dot{m}_{\text{bleed}}$ is bleed mass flow rate, ρ_1 is free-stream density, U_1 is free-stream velocity, and A_b is base area. Simulation results are shown in Figs. 6–12.

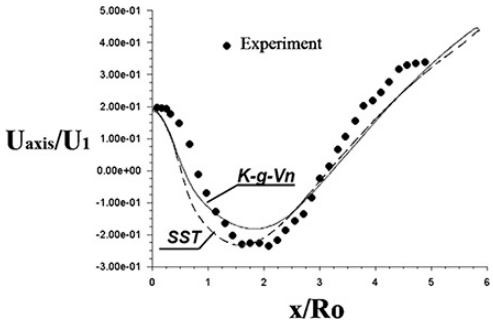

FIG. 6: Mean axial velocities along the centerline. Experimental data by Mathur and Dutton (1996).

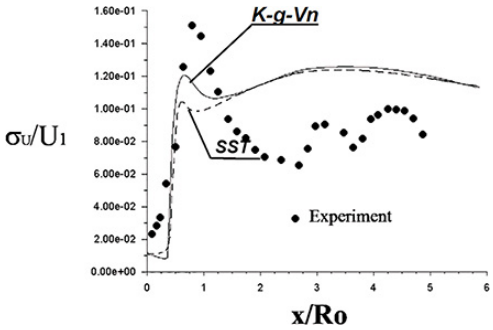

FIG. 7: Axial turbulence intensity along the centerline. Experimental data by Mathur and Dutton (1996).

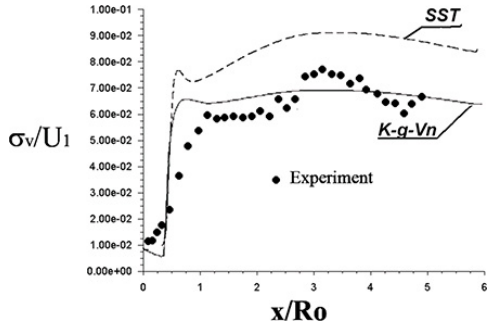

FIG. 8: Radial turbulence intensity along the centerline. Experimental data by Mathur and Dutton (1996).

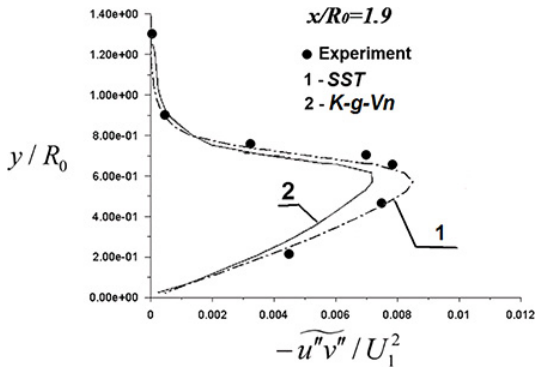

FIG. 9: Normalized Reynolds shear stress vs. radial coordinate at $x_0/R_0 = 1.9$. Experimental data by Mathur and Dutton (1996).

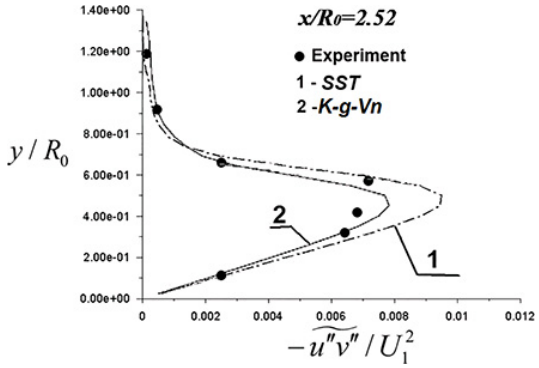

FIG. 10: Normalized Reynolds shear stress vs. radial coordinate at $x_0/R_0 = 2.52$. Experimental data by Mathur and Dutton (1996).

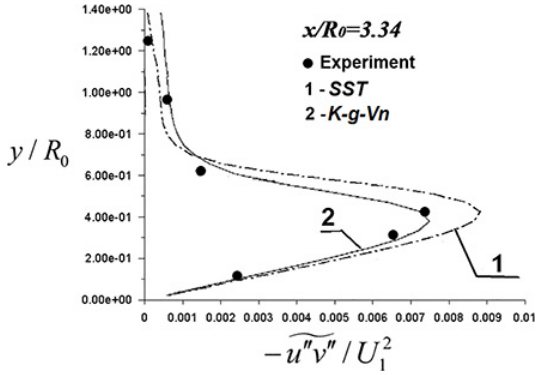

FIG. 11: Normalized Reynolds shear stress vs. radial coordinate at $x_0/R_0 = 3.34$. Experimental data by Mathur and Dutton (1996).

Comparing the simulation results with experimental data shows that the compressibility has more impact on the cross-stream turbulence intensity than on the streamwise one. As one can see, the presented K-g-V_n model gives better or at least none the worse predictions compared to the SST model.

Other compressible flow test cases performed with the model are not presented here for the sake of brevity.

Results for incompressible flows are not presented as well. However, one can easily deduce that at low-speed limit, the present model will probably behave similarly to the SST model in boundary layers, and similarly to v^2-f in free stream conditions. Nevertheless, the issue may need further investigation.

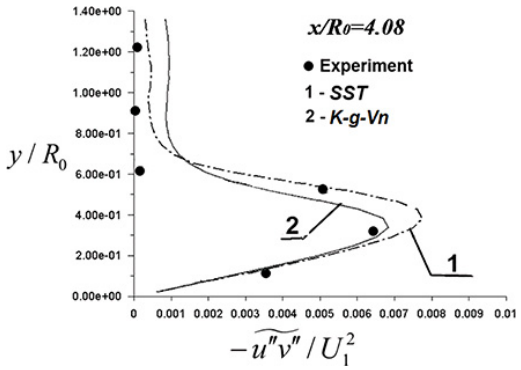

FIG. 12: Normalized Reynolds shear stress vs. radial coordinate at $x_0/R_0 = 4.08$. Experimental data by Mathur and Dutton (1996).

5. CONCLUSION

The developed model gives good agreement with the test data for different flow cases in a wide range of flow parameters and is rather numerically stable and easy to handle, which makes it useful for general engineering applications. In this model, the ideas used in v^2-f, SST, and K-g models are utilized. However, the present model lacks several disadvantages of the latter, like problems with isotropy and boundary condition definition.

REFERENCES

Bertsch, R., Rapidly Sheared Compressible Turbulence: Characterization of Different Pressure Regimes and Effect of Thermodynamic Fluctuations, MS, Texas A&M University, Texas, USA, 2010.

Blaisdell, G.A., Mansour, N.N., and Reynolds, W.C., Compressibility Effects on the Growth and Structure of Homogeneous Turbulent Shear-Flow, *J. Fluid Mech.*, vol. **256**, pp. 443–485, 1993.

Durbin, P.A., Near-Wall Turbulence Closure Modeling without Damping Functions, *Theor. Comput. Fluid Dyn.*, vol. **3**, no. 1, pp. 1–13, 1991.

Dutton, J.C. and Addy, A.L., Fluid Dynamic Mechanisms and Interactions within Separated Flows, U.S. Army Research Office Research Grant DAAH04-93-G-0226, Department of Mechanical and Industrial Engineering, University of Illinois, Urbana-Champagne, Urbana, IL, 1998.

Fernholz, H.H. and Finley, P.J., *A Critical Compilation of Compressible Turbulent Boundary Layer Data*, no. 223, Neuilly-sur-Seine, France: AGARD, 1977.

Freund, J.B., Lele, S.K., and Moin, P., Compressibility Effects in a Turbulent Annular Mixing Layer, Part 1, Turbulence and Growth Rate, *J. Fluid Mech.*, vol. **421**, pp. 229–267, 2000.

Glebov, G.A. and Molchanov, A.M., Model of Turbulence for Supersonic Reacting Jets, *Investigation of Heat Transfer in Flying Vehicles (Issledovanie Teploobmena v Letatelnykh Apparatakh)*, Moscow, Russia: Moscow Aviation Institute, pp. 6–11, 1982.

Goebel, S.G. and Dutton, J.C., Experimental Study of Compressible Turbulent Mixing Layers, *AIAA J.*, vol. **29**, no. 4, pp. 538–546, 1991.

Gomez, C.A. and Girimaji, S.S., Algebraic Reynolds Stress Model (ARSM) for Compressible Shear Flows, AIAA Paper 2011-3572, p. 14, 2011.

Hossain, M.S., Mathematische Modellierung von Turbulenten Auftriebstromungen, PhD, University of Karlsruhe, Karlsruhe, Germany, 1980.

Huang, S. and Fu, S., Modelling of Pressure-Strain Correlation in Compressible Turbulent Flow, *Acta Mech. Sin.*, vol. **24**, pp. 37–43, 2008.

Jones, R.M., Advanced Turbulence Modeling for Industrial Flows, PhD, Louisiana State University, Louisiana, USA, 1996.

Kalitzin, G., Gould, A.R.B., and Benton, J.J., Application of Two-Equation Turbulence Models in Aircraft Design, AIAA Paper 96-0327, p. 14, 1994.

Kline, S.J., Cantwell, B.J., and Lilley, G.M., Eds., *1980-1981 AFOSR-HTTM-Stanford Conference on Complex Turbulent Flows*, Stanford, CA: Stanford University Press, 1981.

Kollmann, W., Ed., *Prediction Methods for Turbulent Flows*, Washington, DC: Hemisphere Publishing Corporation, 1980.

Kraev, V.M. and Yanyshev, D.S., *Unsteady Turbulent Flows in Channels of Powerplants*, Krasnoyarsk, Russia: Siberian State Aerospace University, 2014.

Krasotkin, V.S., Myshanov, A.I., Shalaev, S.P., Shirokov, N.N., and Yudelovich, M.Y., Investigation of Supersonic Isobaric Submerged Turbulent Jets, *Fluid Dyn.*, vol. **23**, no. 4, pp. 529–534, 1988.

Lau, J.C., Morris, P.J., and Fisher, M.J., Measurements in Subsonic and Supersonic Free Jets Using a Laser Velocimeter, *J. Fluid Mech.*, vol. **63**, no. 1, pp. 1–27, 1979.

Lavin, T.A., Reynolds and Favre-Averaged Rapid Distortion Theory for Compressible, Ideal-Gas Turbulence, MS, Texas A&M University, Texas, USA, 2007.

Ljuboja, M. and Rodi, W., Calculation of Turbulent Wall Jets with an Algebric Reynolds Stress Model, *J. Fluid Eng.*, vol. **102**, pp. 350–356, 1980.

Manceau, R. and Hanjalic, K., Elliptic Blending Model: A New Near-Wall Reynolds-Stress Turbulence Closure, *Phys. Fluids*, vol. **14**, no. 2, pp. 744–754, 2002.

Mathur, T. and Dutton, J.C., Base-Bleed Experiments with a Cylindrical Afterbody in Supersonic Flow, *J. Spacecraft Rockets*, vol. **33**, no. 1, pp. 30–37, 1996.

Menter, F.R., Two-Equation Eddy-Viscosity Turbulence Models for Engineering Applications, *AIAA J.*, vol. **32**, no. 8, pp. 1598–1605, 1994.

Molchanov, A.M., A Calculation of Supersonic Non-Isobaric Jets with Compressibility Corrections in a Turbulence Model, Vestnik MAI, vol. **16**, no. 1, pp. 38–48, 2009.

Molchanov, A.M. and Bykov, L.V., Three-Equation K-ε-V_n Turbulence Model for High-Speed Flows, AIAA Paper 2013-3181, p. 30, 2013.

Pantano, C. and Sarkar, S., a Study of Compressibility Effects in the High Speed Turbulent Shear Layer Using Direct Simulation, *J. Fluid Mech.*, vol. **451**, pp. 329–371, 2002.

Papamoschou, D. and Roshko, A., The Compressible Turbulent Shear Layer: An Experimental Study, *J. Fluid Mech.*, vol. **197**, pp. 453–477, 1988.

Sarkar, S., The Stabilizing Effect of Compressibility in Turbulent Shear Flow, *J. Fluid Mech.*, vol. **282**, pp. 163–186, 1995.

Sarkar, S., Erlebacher, G., and Hussaini, M.Y., Compressible Homogeneous Shear: Simulation and Modeling, NASA Contractor Report 189611 92-6, ICASE, 1992.

Sarkar, S., Erlebacher, G., Hussaini, M.Y., and Kreiss, H.O., The Analysis and Modeling of Dilatational Terms in Compressible Turbulence, U.S. Army Research Office Research Grant Report No. ICASE-89-79, NAS 1.26:181959, NASA-CR-181959, NASA Langley Research Center, 1989.

Simone, A., Coleman, G., and Cambon, C., The Effect of Compressibility on Turbulent Shear Flow: A Rapid-Distortion-Theory and Direct Numerical-Simulation, *J. Fluid Mech.*, vol. **330**, pp. 307–338, 1997.

Vreman, A.W., Sandham, N.D., and Luo, K.H., Compressible Mixing Layer Growth Rate and Turbulence Characteristics, *J. Fluid Mech.*, vol. **320**, pp. 235–258, 1996.

Zeman, O., Dilatation Dissipation: The Concept and Application in Modeling Compressible Mixing Layer, *Phys. Fluids A*, vol. **2**, pp. 178–188, 1990.